Elastic Limit and Strain Hardening of Thin Wires in Torsion

D. J. Dunstan,[1,*] B. Ehrler,[1] R. Bossis,[2] S. Joly,[3] K. M. Y. P'ng,[4] and A. J. Bushby[4]

[1]*Centre for Materials Research and Department of Physics, Queen Mary University of London, London E1 4NS, United Kingdom*
[2]*Laboratoire de Génie des Matériaux et Procédés Associés, Ecole Polytechnique de l'Université de Nantes, rue Christian Pauc, 44306 Nantes, France*
[3]*CEFIPA Engineering School, 116 Avenue Aristide Briand, 92220 Bagneux, France*
[4]*Centre for Materials Research and Department of Materials, School of Engineering and Materials Science, Queen Mary University of London, London E1 4NS, United Kingdom*

(Received 10 December 2008; revised manuscript received 18 June 2009; published 5 October 2009)

A theory for the size effect in the strength of wires under torsion is reported and compared with data from thin copper wires. Critical thickness theory is solved rigorously and used to validate a useful approximation which is combined with slip-distance theory modified for a finite structure size. Experimental data with high accuracy around and above the elastic limit show excellent agreement with the theory. The results strongly imply that the physical principle is the constraint that size, whether grain size or structure size, puts on allowed dislocation curvature.

DOI: 10.1103/PhysRevLett.103.155501 PACS numbers: 62.20.F−, 46.35.+z

It is well established in semiconductor technology that thin structures such as epitaxial strained layers can be very much stronger than bulk material [1–3]. Size-effect strengthening is also observed in many other materials and experimental situations. As well as the classic Hall-Petch effect in which smaller grain sizes lead to higher strength [4], size effects are seen in nanoindentation [5], in twisting thin wires [6], bending thin foils [7], and compressing small pillars [8]. Understanding size effects is important at low strain in the vicinity of the elastic limit, since structural failure (whether by fracture, creep or fatigue) is usually a consequence of exceeding the elastic limit. Understanding size effects is also important at high strain in the context of metrology using indentation hardness testing and nanoindentation.

Theories of these effects have generally invoked indirect effects of the size. These include obstruction of dislocation passage by grain boundaries leading to pileup [4,9], dislocation annihilation at free surfaces leading to dislocation starvation [10], and various forms of strain gradient theory in which it is not the size *per se* but the gradient of plastic strain that matters [6,7,11–13]. In fact, finite size in itself can be sufficient to account directly for increased strength. Here we show how finite size acts through critical thickness effects [1–3,14], and through a closely related physically necessary modification of Taylor (forest) strain hardening. In both cases the size effect arises through the size constraint on dislocation curvature. We present experimental data on the torsion of thin wires in good agreement with these ideas.

Conrad considered plastic flow as the passage of dislocations through a crystal leading to an average plastic strain dependent on the mean free path of dislocations. He introduced this "slip-distance" theory to explain the Hall-Petch effect [15,16]. Then the plastic strain $\varepsilon_{\mathrm{pl}}$ is given by the density of mobile dislocations, assumed to be some fraction of the total density, $\rho_m = \lambda\rho$, and by their mean free path $\bar{x}$, assumed to be some fraction of the grain size, $\bar{x} = \xi d$, so that

$$\varepsilon_{\mathrm{pl}} = b\bar{x}\rho_m = b\xi d\lambda\rho, \tag{1}$$

where b is the effective Burger's vector of relevant dislocations and λ and ξ are dimensionless fractions of the order of unity. The flow stress is determined by forest strain-hardening (often incorrectly called Taylor strain-hardening) [17,18].

$$\sigma = \alpha G b\sqrt{\rho} = \alpha G\sqrt{\frac{b\varepsilon_{\mathrm{pl}}}{\lambda\xi d}}, \tag{2}$$

where α is the Taylor coefficient, of the order of unity for forest strain hardening. In this form, slip-distance theory gives the observed Hall-Petch inverse-square-root dependence of flow strength on grain size, but gives no dependence on structure size. If we replace the grain size d by the structure size h in Eq. (1) we obtain an inverse-square-root dependence of flow strength on structure size, but we lose the dependence on grain size. Experimental results show that both are needed [19].

To incorporate both grain size and structure size in the theory, consider an infinite line along which the linear density or spatial frequency of randomly placed points X is $\rho_x = x^{-1}$ where x is the average interval. Let a second set of points Y be added with $\rho_y = y^{-1}$. Starting from a randomly chosen origin, the probability per unit distance of encountering a point is $\rho_{xy} = \rho_x + \rho_y = x^{-1} + y^{-1}$. So between two free surfaces separated by the structure size h and with grain boundaries separated by d on average, the appropriate value of slip distance in Eq. (1) is $\bar{x} = \xi(h^{-1} + d^{-1})^{-1}$. Similarly, for the average spacing between dislocations, $\sqrt{\rho}$ in Eq. (2), becomes $\ell_{\mathrm{eff}}^{-1} = \sqrt{\rho} + L^{-1} = \sqrt{\rho} + h^{-1} + d^{-1}$. Using these modifications, and eliminat-

ing stress by using $\sigma = G\varepsilon_{\rm el}$, we express slip-distance theory as

$$\begin{aligned} \varepsilon_{\rm pl} &= b\bar{x}\rho_m = b\xi(h^{-1} + d^{-1})^{-1}\lambda\rho \\ \varepsilon_{\rm el} &= \alpha b(\sqrt{\rho} + h^{-1} + d^{-1}) \qquad \varepsilon_{\rm pl} + \varepsilon_{\rm el} = \varepsilon. \end{aligned} \tag{3}$$

These three equations can be solved analytically for $\varepsilon_{\rm pl}(\varepsilon)$. Unlike Eq. (2), they predict a nonzero yield strength or elastic limit at $\varepsilon_{\rm pl} = \rho = 0$. For small structures, however, it is not clear that Eq. (3) gives an adequate description of the strength for the very first dislocation, nor what role strain gradient might play, nor whether dislocation sources can operate within the size constraints. A clearer picture of the onset of plastic deformation and the operation of sources is given by critical thickness theory [1–3], which we now calculate explicitly for a wire in torsion.

Consider a wire of infinite length and radius a under torsion, leading to a shear strain at radius r of κr where κ is the twist per unit length. Following Matthews [1], we introduce a suitable dislocation and consider whether it will extend indefinitely to relieve strain throughout the length of the structure. This is an edge dislocation on a diameter of the wire, shown in Fig. 1, curve (a), with a Burger's vector b in the z direction and with a glide plane along the length of the wire. We assume that the crystallography permits this. Under the torsional shear stress there is a force on the dislocation which causes it to curve as shown in Fig. 1, curve (b), and if the force is sufficient the dislocation will extend indefinitely leaving a screw dislocation along the axis of the wire as in Fig. 1, curve (c). Following the Matthews approach [1–3], we calculate the total elastic energy with and without the axial screw dislocation, and critical values of κ or a are the values for which these energies are equal. The shear strain due to the axial screw dislocation is $-b/(2\pi r)$ which diverges as r goes to 0 and so we introduce a core cutoff radius r_0. Then the elastic energy per unit length without the dislocation is

$$U_e = \frac{1}{2}G\int_{r=r_0}^{a} 2\pi r(\kappa r)^2 dr = \frac{1}{4}\pi G\kappa^2(a^4 - r_0^4). \tag{4}$$

The energy with the dislocation is

$$\begin{aligned} U_R &= \frac{1}{2}G\int_{r=r_0}^{a} 2\pi r\left(\kappa r - \frac{b}{2\pi r}\right)^2 dr \\ &= \frac{1}{4}\pi G\kappa^2\left((a^4 - r_0^4) - \frac{2b(a^2 - r_0^2)}{\kappa\pi} + \frac{b^2\ln(a/r_0)}{\pi^2\kappa^2}\right). \end{aligned} \tag{5}$$

Equating U_e and U_R and solving for κ, we get the critical twist per unit length as

$$\kappa_c = \frac{b}{2\pi(a^2 - r_0^2)}\ln\frac{a}{r_0} \approx \frac{b}{2\pi a^2}\ln\frac{a}{b}, \tag{6}$$

where the approximate expression has $r_0 = 0$ except within the logarithmic term and $r_0 = b$ within it. There is a massive literature on critical thickness theory and many refinements can be applied to Eq. (6) [2]. For practical applications in strained-layer epitaxy, we introduced a geometrical approximation, in which misfit dislocations are favored at a depth h below a free surface if the integrated excess strain-thickness product above h exceeds the Burgers vector b [3,20]. From Eq. (6), approximating the logarithmic term to 10 for $a \sim \mu$m, $r_0 = b \sim$ Å, we have the integrated strain-thickness product at the critical twist of

$$\int_{r=0}^{a}\frac{r}{a}\kappa_c dr = \int_{r=0}^{a}\frac{10b}{2\pi a}\frac{r}{a}dr = \frac{5}{2\pi}b, \tag{7}$$

which is close to b. This is useful, as the geometrical theory was developed for flat surfaces [20] and it was not clear if it is valid for curved surfaces as in a wire in torsion [14].

At the critical twist, the termination of the misfit dislocation curves sufficiently to reach the surface at right angles [Fig. 1, curve (c)]. If dislocation sources are required to operate, 4 or 5 times as much dislocation curvature is required, as shown schematically in Fig. 1, curve (d), so the critical strain-thickness product becomes $\sim 4b$ or $5b$. A Frank-Read source is shown, for which the condition is that each of the five quarter-circles making it up requires an excess strain-thickness product of b [3]. The theory above is unaltered except for rescaling the required excess strain-thickness integral from b to $5b$. We will use both values: b for establishing the elastic limit, and $5b$ to fit data at larger plastic strains where dislocation sources must operate.

In previous wire-torsion experiments, Fleck *et al.* reported no data below $\varepsilon_{\rm pl} \sim 0.01$, far above the elastic limit [6]. They used 2 mm gauge lengths and they measured the torque. To obtain data complementary to theirs, we use much longer gauge lengths up to 1 m, and we use a load-

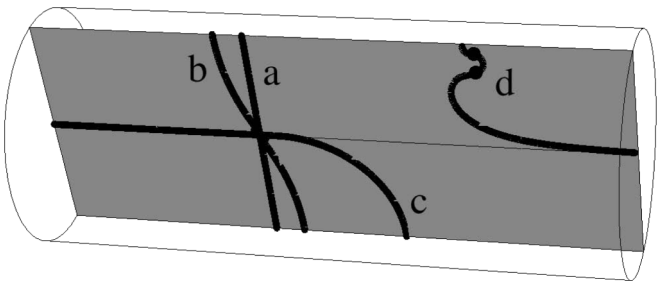

FIG. 1. Part of a long cylinder or wire is shown. A diametrical edge dislocation with Burgers vector parallel to the axis of the cylinder is marked (a). Under torsion, it curves as shown (b), keeping the ends of the segment perpendicular to the free surfaces. Once the critical condition is reached, the dislocation extends indefinitely by glide of the end segments, one of which is shown at (c). "Misfit" or "geometrically necessary" screw dislocation is thus generated on the axis of the cylinder. At 5 times the critical condition, the easiest Frank-Read source, shown at (d), can begin to operate.

unload technique instead of measuring the torque [7,19,21]. Copper wires of diameter 10 and 50 μm were wound on a bobbin and annealed in a rapid thermal annealing furnace to give a range of grain sizes. Grain sizes were measured by focused ion-beam secondary-electron scanning microscopy, counting the number of grains along a line of specified length on images of the cylindrical surface of the wire or on images of flat surfaces made by focused ion-beam milling. The average grain sizes reported here are only approximate (± 1 μm) but they are certainly good enough for our purposes. Texture was also measured and found to be substantially isotropic.

Lengths of wire were suspended vertically ($L = 1$ m for 50 μm and $L = 0.26$ m for 10 μm diameter wire) and a low-mass crossbar was fixed at the bottom. In order to anneal out any strain-hardening due to handling, electrical heating in a nitrogen atmosphere to about 300 °C–400 °C was used before taking data. More experimental details are given in the supplementary online material [22].

A turntable with a pair of pins engaging with the crossbar was used to twist the wires to various twist angles φ_L, the ''load'' condition. After each successive value of φ_L, the turntable was backed off until the wire hung freely. The angles of the crossbar in this ''unload'' condition, φ_U, were measured to an accuracy of 0.05 radians. The data plotted in Fig. 2 are for a single 10 μm wire and two 50 μm wires, one measured under the same conditions as the 10 μm wire (open triangles) and the other with some improvements to the experiment for greater accuracy at the lowest strains. The two steps in the latter dataset at 6 and 12 rad are due to 10 min pauses under load to test for creep.

If $\varphi_U = 0$, the deformation at φ_L was wholly elastic or reversible. Key points to note in Fig. 2 are that φ_U is indeed zero within experimental error up to a clear elastic limit, and the elastic limit is much higher in the thinner wire. When there is plastic strain $\varepsilon_{\rm pl}(r)$, it is easy to show that the unload angle φ_U is

$$\varphi_U = \frac{4L}{a^4}\int_{r=0}^{a} r^2 \varepsilon_{\rm pl}(r) dr \tag{8}$$

To fit to the data, first, we add an intrinsic yield strength ε_0 to the expression for $\varepsilon_{\rm el}$ [Eq. (3)] to take account of, e.g., the Peierls stress. Then we substitute φ_L for κL throughout. We calculate the radius at which the elastic strain equals the elastic limit implicit in Eq. (3), given by

$$r_{\rm elm} = \frac{L}{\varphi_L}[\varepsilon_0 + \alpha b(a^{-1} + d^{-1})]. \tag{9}$$

The radius above which the excess strain-thickness product equals $5b$ is given by

$$1/2\kappa(a - r_{\rm ct})^2 = 5b \Rightarrow r_{\rm ct} = a - \sqrt{\frac{10bL}{\varphi_L}}, \tag{10}$$

and according to critical thickness theory the plastic deformation $\varepsilon_{\rm pl}(r)$ is constant for r from $r_{\rm ct}$ to a [14].

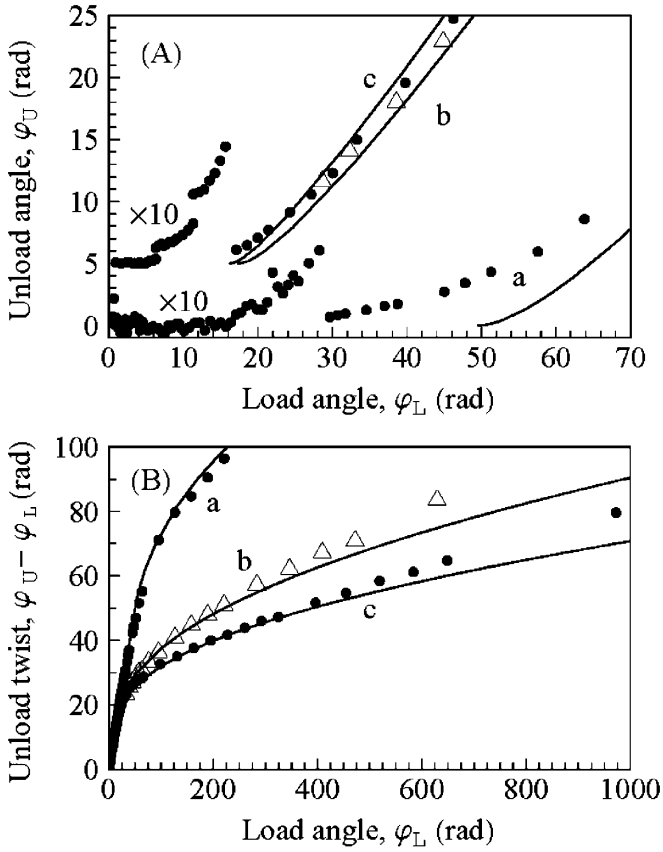

FIG. 2. Load-unload data in torsion is shown for three wires, (*a*) a 10 μm diameter wire with an average grain size of $d = 11$ μm and length 0.26 m, (*b*) a 50 μm diameter wire with an average grain size of $d = 8.4$ μm and length 1 m (open triangles), and (*c*) a 50 μm diameter wire with an average grain size of $d = 21$ μm and length 1 m. In the upper panel (a), the data at very low strain is shown, with φ_U plotted against φ_L. The data for (*b*) and (*c*) are offset by five radians on the φ_U axis for clarity, and are multiplied by ten on the φ_U axis up to load angles of 28 rad (*a*) and 17 rad (*c*) to show the elastic limit more clearly. Elastic limits of $\varphi_L = 16$ rad (*a*) and 5 rad (*c*) are visible in the data. The breakpoints at 6 and 11 rad in the data of (*c*) are due to pauses under load to test for creep. In the lower panel (b), the full range of data is plotted as $\varphi_L - \varphi_U$ against φ_L similar to a stress-strain plot. The solid curves in both panels are fits using Eq. (3) and (11) with parameter values given in the text.

Dislocation sources start to operate when $\varphi_L = \varphi_{L0}$ such that $r_{\rm elm} = r_{\rm ct}$. Single axial dislocations are favored under the same condition when b instead of $5b$ is used in Eq. (10), defining φ_{LS}. Then, using the solution of Eq. (3) for $\varepsilon_{\rm pl}(\varepsilon)$ and substituting $\varphi_L r/L$ for ε,

$$\varphi_U(\varphi_L) = \frac{4L}{a^4}\left(\int_{r_{\rm elm}}^{r_{\rm ct}} r^2 \varepsilon_{\rm pl}(r) dr + \int_{r_{\rm ct}}^{a} r^2 \varepsilon_{\rm pl}(r_{\rm ct}) dr\right). \tag{11}$$

This integral can be evaluated analytically, but the analytic expression is much too lengthy to be useful. Putting numbers in, we therefore calculate the fits to data which are given in Fig. 2. The magnitude of the Burgers vector of

copper is taken to be 0.256 nm. The intrinsic strength and the dimensionless parameters of the order of unity have been adjusted to obtain the best fit ($\varepsilon_0 = 1.8 \times 10^{-4}$, $\alpha = 1$, the product $\lambda\xi = 0.4$, and the coefficients of h^{-1} and d^{-1} in Eq. (3) were also left at unity). The fit is excellent at the higher strains [lower panel, Fig. 2(b)]. At the lowest plastic strains [upper panel, Fig. 2(a)], we expect plasticity to initiate at φ_{LS} rather than φ_{L0} and the inhomogeneity of the wire (distribution of grain sizes) will smooth what would otherwise be stepwise plastic deformation.

It is unlikely that the fit of Fig. 2 is unique. Two reservations should be noted. Critical thickness theory was developed for epitaxial crystal on nearly perfect substrate and explains the elastic limit and the onset of the operation of sources. The application to the much lower-quality structures here is speculative but seems to be necessitated by the increased elastic limit of the thinner wire. Unquestionably, a more comprehensive and detailed microscopic characterization of the specimens before test could help validate the model and perhaps help explain the results at the lowest plastic strains. However, it is highly significant that a good fit can be obtained with physically plausible values for the fitting parameters in wires of different diameters and in wires of the same diameter and different grain sizes. It is also highly significant that the only parameters describing the specimens are the Burgers vector of copper, and the measured diameters and average grain sizes. This implies (a) that other metallurgical parameters such as texture are either unimportant or consistent with our assumptions, and (b) that the theory should work for other strain conditions such as foil bending or simple tension and for other metals, without needing to change the dimensionless parameters. There remain many other unanswered questions, e.g., whether the theory presented here should be applied to precreep or to postcreep data. Experiments over a wider range of grain sizes and wire diameters, and to much higher strain and a range of load times, are clearly urgent. Meanwhile, these results already strongly imply that the physical principle determining the elastic limit and early strain hardening of a soft metal is the constraint that size, whether grain size or structure size, puts on allowed dislocation curvature.

*Corresponding author.
d.dunstan@qmul.ac.uk

[1] J. W. Matthews, Philos. Mag. **13**, 1207 (1966).
[2] E. A. Fitzgerald, Mater. Sci. Rep. **7**, 87 (1991).
[3] D. J. Dunstan, J. Mater. Sci. Mater. Electron. **8**, 337 (1997).
[4] E. O. Hall, Proc. Phys. Soc. London **64**, 747 (1951); N. J. Petch, J. Iron Steel Inst. **174**, 25 (1953).
[5] T. T. Zhu, A. J. Bushby, and D. J. Dunstan, J. Mech. Phys. Solids **56**, 1170 (2008).
[6] N. A. Fleck *et al.*, Acta Metall. Mater. **42**, 475 (1994).
[7] J. S. Stölken and A. G. Evans, Acta Mater. **46**, 5109 (1998).
[8] M. D. Uchic *et al.*, Science **305**, 986 (2004).
[9] J. C. M. Li and Y. T. Chou, Metall. Trans. **1**, 1145 (1970).
[10] J. R. Greer and W. D. Nix, Phys. Rev. B **73**, 245410 (2006).
[11] M. F. Ashby, Philos. Mag. **21**, 399 (1970).
[12] R. de Borst and H.-B. Mühlhaus, Int. J. Numer. Methods Eng. **35**, 521 (1992).
[13] H. Gao, Y. Huang, W. D. Nix, and J. W. Hutchinson, J. Mech. Phys. Solids **47**, 1239 (1999).
[14] D. J. Dunstan and A. J. Bushby, Proc. R. Soc. A **460**, 2781 (2004).
[15] H. Conrad, S. Feuerstein, and L. Rice, Mater. Sci. Eng. **2**, 157 (1967).
[16] K.-H. Chia, K. Jung, and H. Conrad, Mater. Sci. Eng. A **409**, 32 (2005).
[17] G. I. Taylor, Proc. R. Soc. A **145**, 362 (1934).
[18] N. F. Mott, Proc. R. Soc. A **220**, 1 (1953).
[19] B. Ehrler *et al.*, Thin Solid Films **517**, 3781 (2009).
[20] D. J. Dunstan, S. Young, and R. H. Dixon, J. Appl. Phys. **70**, 3038 (1991).
[21] B. Ehrler *et al.*, Philos. Mag. **88**, 3043 (2008).
[22] See EPAPS Document No. E-PRLTAO-103-004943 for more details of the specimens and the results. For more information on EPAPS, see http://www.aip.org/pubservs/epaps.html.